Research Article Vol. 37, No. 9 / September 2020 / Journal of the Optical Society of America B 2773

Journal of the Optical Society of America B

OPTICAL PHYSICS

Picostrain-resolution fiber-optic sensing down to sub-10 mHz infrasonic frequencies

Nabil Md Rakinul Hoque* and Lingze Duan

Department of Physics and Astronomy, University of Alabama in Huntsville, Huntsville, Alabama 35899, USA
**Corresponding author: nh0014@uah.edu*

Received 17 April 2020; revised 27 July 2020; accepted 27 July 2020; posted 27 July 2020 (Doc. ID 395397); published 25 August 2020

High-resolution strain sensing based on long, high-finesse fiber Fabry–Perot interferometers (FFPIs) has been demonstrated with a special focus on the infrasonic frequency range. A novel dual-FFPI scheme allows the large environment-induced background at low frequencies to be suppressed, permitting high strain resolution limited only by excess electronic noise. Noise-equivalent strain resolution of 257 pε/√Hz has been achieved at 6 mHz, and the resolution improves to ∼200 fε/√Hz between 4–20 Hz. Without the use of any additional optical frequency references and with only off-the shelf commercial components, these resolutions are much better than most in the prior reports. Especially, an improvement of a factor of 1.8 is achieved in comparison with the highest resolution reported so far near 5 Hz. The limiting factors of the current scheme have been analyzed in detail, and the application prospects have been demonstrated using an acoustic transducer. The work lays out the potential of using long FFPIs with high finesse for high-resolution fiber-optic sensing in the infrasonic frequency range.

https://doi.org/10.1364/JOSAB.395397

1. INTRODUCTION

Sensors operating at infrasonic frequencies (typically between 1 mHz and 20 Hz) have become increasingly important in recent years because of their potential applications in mass-destruction weapon detection, structural health monitoring, oil and gas exploration, as well as seismology and geophysics [1–4]. In many cases, optical fiber sensors are preferred over other types of sensors due to the superiority of fibers in cost, flexibility, durability, immunity to electromagnetic (EM) interference, and feasibility to multiplex a large number of sensors [5].

High-resolution, fiber-optic sensors capable of operating at infrasonic frequencies have been the topic of several recent reports [6–12]. Notably, using a single fiber Bragg grating (FBG) sensor, Arie *et al.* demonstrated a 1.2 nε/√Hz strain resolution at 1.5 Hz by locking the interrogation laser to an atomic absorption line [6]. The sensitivity of FBG-based sensors can be enhanced by inserting a $\lambda/4$ gap in the middle of the gratings, which creates a sharp notch orders of magnitude narrower than a normal Bragg reflection peak (tens of megahertz versus a few gigahertz) [7]. Using such π-phase-shifted FBGs, Chen *et al.* achieved a better strain resolution of 0.4 nε/√Hz within 0.01–50 Hz [8]. An alternative approach of generating ultra-narrow resonance peaks is to utilize long fiber Fabry–Perot interferometers (FFPIs) [9]. For example, Lam *et al.* demonstrated strain resolutions as low as 2 nε/√Hz at frequencies down to 10 mHz and 6 pε/√Hz at frequencies above 2 Hz using an FFPI sensor (5 cm cavity length with a finesse of ∼20) interrogated with a diode laser frequency-locked to an $H_{13}C_{14}N$ absorption line [10]. Littler *et al.* also devised an FFPI-based sensing system with pico-strain level resolution in the infrasonic regime down to 4 Hz [11]. Meanwhile, a notable achievement was made by Gagliardi *et al*., who reported strain resolutions of 350 fε/√Hz at 5 Hz and 20 pε/√Hz at 50 mHz by interrogating a 13-cm FFPI with a diode laser frequency-referenced to an optical frequency comb (OFC) [12].

Passive fiber-optic sensing in the infrasonic region faces unique challenges compared to sensing at higher frequencies. Since laser frequency noise (FN) is the predominant noise source for interferometric optical sensors [13,14], the rapid roll-up of laser noise spectrum at the low-frequency end, usually due to large random frequency drift, can cause a rapid reduction of resolution as the frequency approaches zero. This is the reason why most high-resolution infrasonic sensors reported so far are based on lasers frequency-locked to highly stable frequency references such as atomic transition lines and OFC [6,10,12]. In addition, the 1/f noise in electronic systems and slow environment-induced fluctuations such as temperature changes also make it more difficult for fiber-optic sensors to resolve small signals at infrasonic frequencies.

In the work reported here, we attempt to address these challenges via a different strategy. Instead of trying to remove all the fluctuations, we let the laser frequency fluctuate in a similar fashion as the environment-induced sensor fluctuation. This allows the large frequency drift of the laser and the large fluctuation of

the sensor to cancel out when the laser is used to interrogate the sensor because they become a common-mode noise. As a result, small infrasonic signals applied on the sensor can be detected.

Specifically, the strain sensor used in this work is a very long (1 m) FFPI with a very high finesse (~1000). It offers the benefit of extremely high-frequency discrimination (~100 kHz linewidth), which translates to a very high strain sensitivity. But at the same time, the narrow operating frequency range also makes it very difficult to directly interrogate the sensor with a laser. Although, in principle, it is possible to frequency-lock a laser to the FFPI and probe it through the lockbox output signal [15,16], the large relative frequency drift between the laser and the FFPI resonance would generate a large background noise floor at the low-frequency end, considerably limiting the achievable resolution in the infrasonic region. To tackle this problem, we have introduced a reference FFPI, which has similar specifications as the sensor FFPI. The two FFPIs are packaged under a similar environment except for the strain transducer, which is a piezoelectric (PZT) actuator mounted on the sensor FFPI. The laser is first frequency-locked to the reference FFPI, which allows its frequency to follow the drift of the FFPI resonance. It is then used to interrogate the sensor FFPI. Since the two FFPI experience similar frequency drift, the relative frequency drift between the laser and the sensor FFPI is significantly reduced, permitting reliable measurement of low-frequency signals. Calibrated strain measurement has been performed at 100 mHz, and noise-limited strain resolution has been characterized in the infrasonic region down to 6 mHz; both are at record-low frequencies to the best of our knowledge.

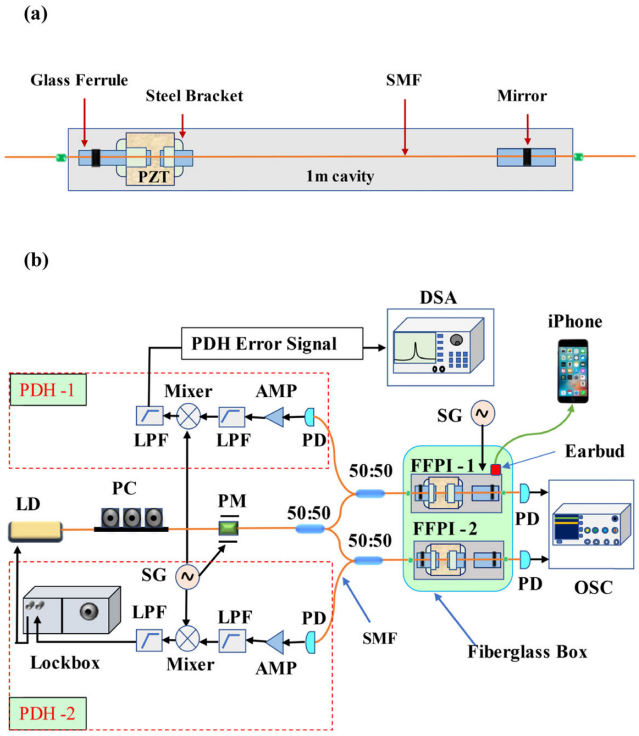

Fig. 1. (a) Schematic of the 1-m-long FFPI sensor. (b) Layout of the experimental setup. Amp, rf amplifier; LD, laser diode; LPF, low-pass filter; PD, photodetector; PM, phase modulator; SG, signal generator; SMF, single-mode fiber; OSC, oscilloscope.

2. EXPERIMENTAL METHOD

The FFPI strain sensor used in our experiment is a commercial fiber Fabry–Perot scanning interferometer (Micron Optics, FFP-SI) with a 1-m cavity length, as shown in Fig. 1(a). Both ends of the FFPI are coated with multilayer high-reflection coatings to attain a manufacturer-specified finesse of 1000. A PZT actuator is installed near one end of the FFPI (inside the assembly) to allow for fine tuning of the cavity length and hence resonance frequencies. It also serves as an infrasonic strain transducer. In addition, for demonstration of acoustic sensing, an earbud is glued on the case of the FFPI (outside the assembly). The sensor assembly is situated in a fiberglass box whose inside wall is lined with sound-absorbing foams. Also packaged inside the fiberglass box is the reference FFPI [FFPI-2 in Fig. 1(b)], which has similar length and finesse as the sensor.

The experimental setup consists of two Pound-Drever-Hall (PDH) systems [17], as shown in Fig. 1(b). They are driven by a common light source, which is a commercial diode laser (RIO, Orion) operating at 1550.05 nm with a 1-kHz linewidth. The PDH system for the reference FFPI [PDH-2 in Fig. 1(b)] is running in close loop, with the output of the lockbox (New Focus LB1005) feeding into the laser controller to lock the laser frequency to a resonance peak of FFPI-2. The effective locking bandwidth is on the order of 10 Hz, allowing the laser frequency to follow the slow drift of the resonance peak without picking up an excessive amount of high-frequency jitter from the resonator. Meanwhile, the PDH system for the FFPI sensor [PDH-1 in Fig. 1(b)] is kept open, with the laser frequency stationed near the center of a resonance peak under the steady state. The PDH error signal is then used as the readout of the strain signal and is analyzed with a fast Fourier-transform dynamic signal analyzer (DSA) (Stanford Research Systems, SR785). Additionally, the optical power transmissions through the two FFPIs are monitored using two photodetectors and an oscilloscope, as illustrated in Fig. 1(b).

3. EXPERIMENTAL RESULT

As previously mentioned, the dual-FFPI scheme significantly reduces the impact of environment-induced fluctuations and hence enables reliable laser interrogation of the long FFPI sensor. This is demonstrated by the fact that the laser frequency can remain stable relative to the resonance peaks of the FFPI sensor for an extended period of time (>30 min) [18]. When a dc voltage is applied on the PZT actuator in the sensor, the relative frequency between the laser and an FFPI resonance peak can be tuned in a controlled fashion. Figure 2 shows the measured PDH-2 error signal (solid) and FFPI-2 transmission (dotted) during this process. The error signal displays a characteristic antisymmetric shape for PDH error signal [17], while the transmission clearly maps out the ~100-kHz-wide resonance peak.

By fixing the laser frequency at the center of a resonance peak of the sensor FFPI, one can exploit the steep linear slope of the PDH error signal (see solid trace in Fig. 2) and use it as a highly sensitive frequency discriminator to measure strain-induced frequency shift. With proper calibration, the actual strain

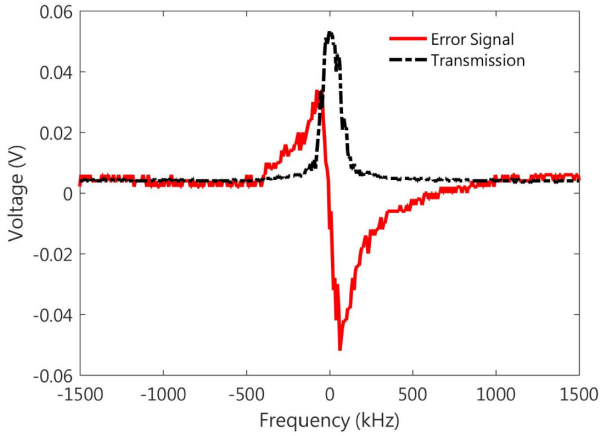

Fig. 2. PDH error signal (solid line) and the corresponding transmission peak (dashed line) of the sensor FFPI are clearly mapped out by scanning the laser frequency across the FFPI resonance in a controlled fashion.

applied on the sensor can be determined. Such measurements have been performed by applying harmonic modulations of different frequencies and amplitudes on the PZT actuator embedded in the FFPI sensor. The calibration is done through manufacturer-specified PZT response. Figures 3(a) and 3(b) show the sensor response spectra under strain modulations of 300 Hz (52-pε amplitude) and 100 mHz (8.5-nε amplitude), respectively. These results demonstrate that the FFPI sensor can operate within a broad range of frequencies. Its capability to reliably measure dynamic strain at very low frequencies is worth particular attention, as this highlights the advantage of the dual-FFPI scheme. Performing the above measurements with different amplitudes leads to an empirical relation between sensor response and the applied strain, which is shown in Fig. 3 for 300-Hz modulation. Such a relation not only validates the effectiveness of the FFPI sensor as a strain-sensing device but

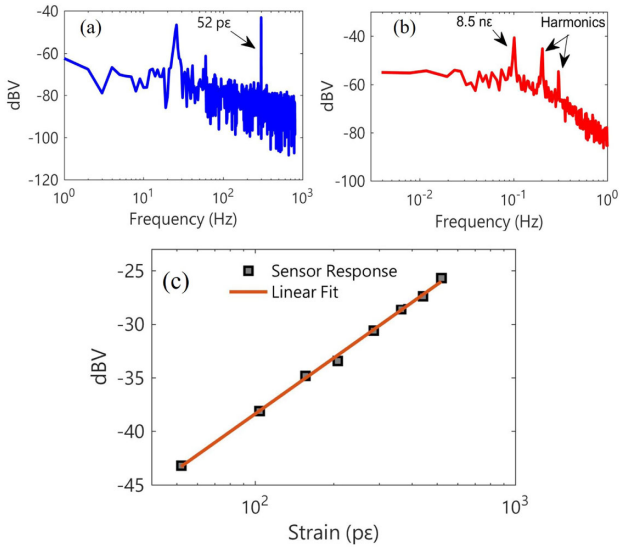

Fig. 3. Strain responses of the FFPI sensor under various excitations. (a) 52 pε at 300 Hz; (b) 8.5 nε at 100 mHz; and (c) with different strain amplitudes (52 − 520 pε) at 300 Hz.

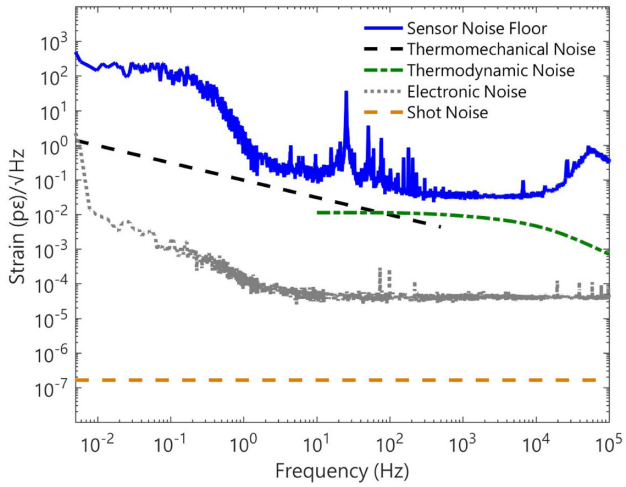

Fig. 4. Noise-equivalent strain resolution of the FFPI sensor from 4 mHz to 100 kHz (solid line) in comparison with fiber thermal noise, including thermomechanical noise (<1 kHz; dashed line) and thermodynamic noise (>10 Hz; dashed-dotted line), electronic noise (dotted line) due to photodetector, rf amplifiers and DSA, as well as shot noise (bottom trace).

also provides a means to determine the noise-limited strain resolution.

The noise-limited strain resolution has been measured over a wide frequency range that extends from infrasonic to ultrasonic frequencies (6 mHz to 100 kHz), as shown in Fig. 4. Strain resolutions as high as 37 fε/$\sqrt{\text{Hz}}$ have been achieved within 1–10 kHz, which is close to the reported resolution of 30 fε/$\sqrt{\text{Hz}}$ at 30 kHz with a *single* FBG [14]. This is because, with a 10-Hz locking bandwidth, the PDH-2 loop is only effective within the infrasonic range. Thus, at high frequencies, the sensor is equivalent to a single FBG. On the other hand, the benefit of the dual-FFPI scheme is in display at the low-frequency end. For example, sub-pε resolution as high as 200 fε/$\sqrt{\text{Hz}}$ is observed in the infrasonic region between 4–20 Hz, which represents an improvement of a factor of 1.8 from the previous best result in the same frequency range [12]. Below 4 Hz, the noise floor experiences a sharp increase before it reaches a plateau at about 100 mHz. The measured strain resolution at 100 mHz is about 150 pε/$\sqrt{\text{Hz}}$, and it has only a mild increase to 257 pε/$\sqrt{\text{Hz}}$ at 6 mHz. To the best of our knowledge, this is the first time dynamic strain resolution is characterized down to the sub-10 mHz level. Although superior resolutions at 50 mHz have been reported [12], it is worthwhile to point out that sophisticated laser frequency stabilization based on an OFC is employed in that work. In comparison, no optical frequency reference is used in the current work and the *off-the-shelf* diode laser is running on its intrinsic linewidth.

There is still room for improvement though. To better understand the limiting factors of the current setup, it is essential to identify the dominating source of the sensor noise floor. Aside from the strain noise floor, shown in Fig. 4 are also the strain-equivalent electronic noise floor (primarily due to the photodetectors, the rf electronics, and the measurement instruments) as well as the estimated spontaneous thermal fluctuation of the optical fiber. The latter has been calculated according to

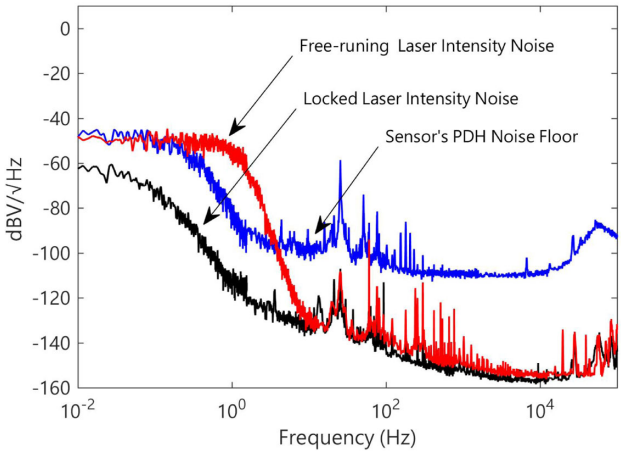

Fig. 5. FFPI sensor noise spectrum in comparison with the laser RIN noise spectra under both free-run and locked (to the reference FFPI) conditions.

both the thermodynamic model [19] and the thermomechanical model [20]. The predictions of the two models are plotted in Fig. 4 based on their dominant frequency ranges [13,21]. These results indicate that the strain noise floor of the sensor is likely limited by other mechanisms.

Prior reports have shown that laser noise often dominates in resonator-based optical sensors [14,22]. Thus, a close examination of the impact of laser noise is necessary. We are especially interested in finding out the sources of the 25-Hz peak and the steep slope between 4 Hz and 100 mHz in the sensor noise floor. Laser noise consists of relative intensity noise (RIN) and FN. Since it is very difficult to independently measure FN, we have chosen to characterize RIN, which is done by directly probing the laser output with a photodetector. Figure 5 shows the measured RIN spectra with the laser operating in both free-run and locked (to FFPI-2) states, along with the sensor noise floor. In all three cases, the optical power incident on the photodetector is kept the same.

A couple of conclusions can be drawn by comparing these three traces. First of all, the existence of the 25-Hz noise peak in the free-running laser RIN suggests that the noise peak likely originates from the laser, possibly due to the driving electronics or the temperature control (TEC) system inside the laser module. Furthermore, the RIN of the locked laser has a similar rising slope between 4 Hz and 100 mHz as the sensor noise floor, indicating that they may share the same origin. Since a PDH error signal is typically sensitive to laser FN but insensitive to laser RIN [17], this similarity suggests that part of the FN of the locked laser, hereafter referred to as the *residual FN*, has a similar spectrum at low frequencies as the RIN. It should also be pointed out that this residual FN is unlikely originated from the laser itself because such FN has been suppressed by the closed PDH-2 loop in Fig. 1(b). It is also unlikely that the residual FN is caused by the environment-induced fluctuation of FFPI-2 (reference FFPI), since such a fluctuation is a common-mode noise between FFPI-1 and FFPI-2 and hence should not appear in the error signal of the PDH-1 loop. Given the above analysis, a likely source for the residual FN is the lockbox of PDH-2. It adds fluctuation to the driving current of the laser through the feedback loop, and this excess fluctuation of the driving current would add *both* FN and RIN to the laser.

4. DISCUSSION

An interesting question worth further investigation is whether the same strain resolution can be achieved with a single meter-long FFPI rather than two FFPIs. To test this scenario, we directly lock the laser to the FFPI sensor and then measure the strain applied on the sensor via the output of the lockbox [12]. It should be noted here that, since the bandwidth of the locking system is on the order of 10 Hz, this method is only valid at low frequencies. Figure 6 shows the strain noise floor of the single-FFPI sensor in comparison with that of the dual-FFPI scheme. The dual-FFPI scheme exhibits clearly better strain resolution across the entire infrasonic region. The reason is quite simple: both the laser and the sensor FFPI carry slow but large frequency drift due to ambient temperature changes and/or fluctuations in the driving electronics. This results in large fluctuations in their relative frequency, especially at low frequencies. In the single-FFPI scheme, such instability leads to a large low-frequency background in the sensor output. With dual FFPIs, however, this background is considerably suppressed because the differential-detection nature of the method allows the relative frequency drift to become a common-mode noise. Similar differential-measurement strategies have been used in the past with FBG sensors to eliminate temperature-induced common-mode noise in static-strain sensing [23]. Differential operation between the reference and the sensor was performed via a computational cross-correlation algorithm, and sensor interrogation was achieved by repetitively sweeping the frequency of a narrow-linewidth tunable laser. In comparison, the dual-FFPI scheme reported here requires only a single-frequency laser, and the PDH technique allows differential detection to be accomplished over a broad frequency range.

Another important aspect is how this dual-FFPI method can be used in field applications. A realistic strategy is to introduce a transducer, which is attached to a portion of the FFPI sensor. Let the transducer be exposed to the field under test (e.g., field of

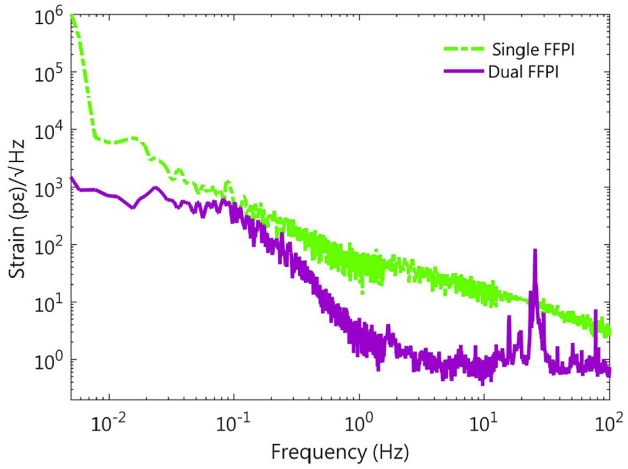

Fig. 6. Comparison between noise-limited strain-resolution spectra for the single-FFPI (dashed-dotted line) and the dual-FFPI (solid line) schemes in the infrasonic frequency region clearly shows the advantage of the dual-FFPI scheme.

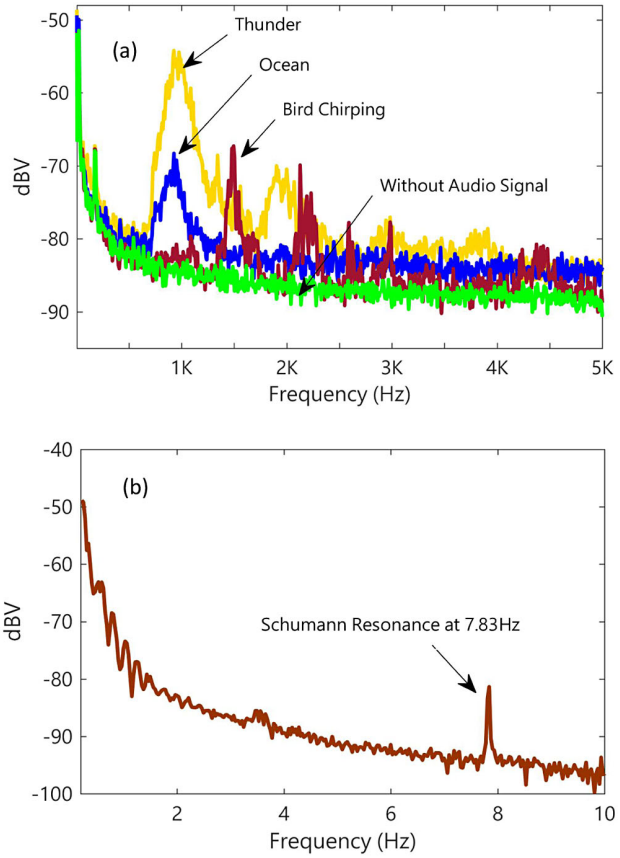

Fig. 7. Demonstration of the application of the FFPI sensor using an acoustic transducer (earbud). (a) Measured spectra of thunder, ocean wave, and bird-chirping sounds; and (b) sensor-detected Schumann-resonance signal at 7.83 Hz.

temperature, pressure, biomolecule samples, etc.) while keeping the rest of the FFPI sensor and the reference FFPI hermetically sealed in the same package. To test the feasibility of this strategy, the earbud attached on FFPI-1 [see Fig. 1(b)] is employed to simulate an acoustic transducer. Various types of acoustic signals are sent to the earbud via an iPhone while the output of the sensor is monitored. Figure 7(a) shows the responses of the sensor under several types of natural sound. The different acoustic characteristics of these sources can clearly be seen in the sensor output. In order to verify the ability of the sensor to detect infrasonic signals, the so-called Schumann resonance is played by the iPhone and sent to the FFPI sensor through the earbud. At 7.83 Hz, the signal is not audible. However, the sensor is able to detect it, as shown in Fig. 7(b).

5. CONCLUSION

In conclusion, a dual-FFPI sensing scheme based on two meter-long, mirror-based, high-finesse fiber FP resonators has shown a great potential in achieving high-resolution strain sensing in the infrasonic frequency range. Calibrated strain measurement has been performed at frequencies as low as 100 mHz, and the ability of the sensor to detect acoustic signals has been demonstrated at both sonic and infrasonic frequencies. A 257-p$\varepsilon/\sqrt{\text{Hz}}$ noise-limited strain resolution has been achieved at 6 mHz. The strain resolution improves to ~200 f$\varepsilon/\sqrt{\text{Hz}}$ between 4–20 Hz and ~37 f$\varepsilon/\sqrt{\text{Hz}}$ between 1–10 kHz. Without relying on any atomic frequency reference or OFC and with only off-the-shelf commercial components, these resolutions are much better than most of the prior reports based on FBG sensors or FBG-based FFPI sensors. The limiting factors of the current scheme have been analyzed in detail and the application prospects have been discussed.

Funding. National Science Foundation (ECCS-1254902, ECCS-1606836); National Aeronautics and Space Administration (80NSSC19M0033); Alabama Graduate Research Scholars Program (Round 14).

Disclosures. The authors declare no conflicts of interest.

REFERENCES

1. J. G. V. Teixeira, I. T. Leite, S. Silva, and O. Frazão, "Advanced fiber-optic acoustic sensors," Photon. Sens. **4**, 198–208 (2014).
2. J. A. Laman and K. M. Reichard, *Long Gage-Length Interferometric Fiber-Optic Sensors for Damage Detection in Bridge Structures* (IDEA Program, Transportation Research Board, 2002).
3. M. A. Zumberge, J. Berger, M. A. H. Hedlin, E. Husmann, S. Nooner, R. Hilt, and R. Widmer-Schnidrig, "An optical fiber infrasound sensor: a new lower limit on atmospheric pressure noise between 1 and 10 Hz," J. Acoust. Soc. Am. **113**, 2474–2479 (2003).
4. P. Ferraro and G. De Natale, "On the possible use of optical fiber Bragg gratings as strain sensors for geodynamical monitoring," Opt. Laser Eng. **37**, 115–130 (2002).
5. F. T. S. Yu and S. Yin, eds., *Fiber Optic Sensors*, Vol. **76** of Optical Engineering (Marcel Dekker, 2002).
6. A. Arie, B. Lissak, and M. Tur, "Static fiber-Bragg grating strain sensing using frequency-locked lasers," J. Lightwave Technol. **17**, 1849–1855 (1999).
7. B. Das, D. Srivastava, U. K. Tiwari, and B. C. Choudhary, "Dynamic strain response of a π-phase-shifted FBG sensor with phase-sensitive detection," OSA Continuum **1**, 1172–1184 (2018).
8. J. Chen, Q. Liu, X. Fan, and Z. He, "Sub-nano-strain multiplexed fiber optic sensor array for quasi-static strain measurement," IEEE Photon. Technol. Lett. **28**, 2311–2314 (2016).
9. E. Udd and W. B. Spillman, Jr., *Fiber Optic Sensors: An Introduction for Engineers and Scientists* (Wiley, 2011).
10. T. T.-Y. Lam, J. H. Chow, D. A. Shaddock, I. C. M. Littler, G. Gagliardi, M. B. Gray, and D. E. McClelland, "High-resolution absolute frequency referenced fiber optic sensor for quasi-static strain sensing," Appl. Opt. **49**, 4029–4033 (2010).
11. I. C. M. Littler, M. B. Gray, J. H. Chow, D. A. Shaddock, and D. E. McClelland, "Pico-strain multiplexed fiber optic sensor array operating down to infra-sonic frequencies," Opt. Express **17**, 11077–11087 (2009).
12. G. Gagliardi, M. Salza, S. Avino, P. Ferraro, and P. D. Natale, "Probing the ultimate limit of fiber-optic strain sensing," Science **330**, 1081–1084 (2010).
13. L. Duan, "Thermal noise-limited fiber-optic sensing at infrasonic frequencies," IEEE J. Quantum Electron. **51**, 7700106 (2015).
14. G. Skolianos, A. Arora, M. Bernier, and M. Digonnet, "Measuring attostrains in a slow-light fiber Bragg grating," in *Slow Light, Fast Light, and Opto-Atomic Precision Metrology IX*, S. M. Shahriar and J. Scheuer, eds. (SPIE, 2016), p. 976317.
15. J. H. Chow, D. E. McClelland, M. B. Gray, and I. C. M. Littler, "Demonstration of a passive subpicostrain fiber strain sensor," Opt. Lett. **30**, 1923–1925 (2005).
16. D. Gatti, G. Galzerano, D. Janner, S. Longhi, and P. Laporta, "Fiber strain sensor based on a π-phase-shifted Bragg grating and the Pound-Drever-Hall technique," Opt. Express **16**, 1945–1950 (2008).

17. R. W. P. Drever, J. L. Hall, F. V. Kowalski, J. Hough, G. M. Ford, A. J. Munley, and H. Ward, "Laser phase and frequency stabilization using an optical resonator," Appl. Phys. B **31**, 97–105 (1983).
18. N. M. R. Hoque and L. Duan, "Direct frequency locking of a diode laser to a meter-long high-finesse fiber Fabry-Perot cavity," in *Conference on Lasers and Electro-Optics* (Optical Society of America, 2019), paper SM1L.4.
19. S. Foster, A. Tikhomirov, and M. Milnes, "Fundamental thermal noise in distributed feedback fiber lasers," IEEE J. Quantum Electron. **43**, 378–384 (2007).
20. L. Z. Duan, "Intrinsic thermal noise of optical fibres due to mechanical dissipation," Electron. Lett. **46**, 1515–1516 (2010).
21. L. Duan, "General treatment of the thermal noises in optical fibers," Phys. Rev. A **86**, 023817 (2012).
22. P. Liu, W. Huang, W. Zhang, and F. Li, "Ultrahigh resolution optic fiber strain sensor with a frequency-locked random distributed feedback fiber laser," Opt. Lett. **43**, 2499–2502 (2018).
23. Q. Liu, T. Tokunaga, and Z. He, "Realization of nano static strain sensing with fiber Bragg gratings interrogated by narrow linewidth tunable lasers," Opt. Express **19**, 20214–20223 (2011).